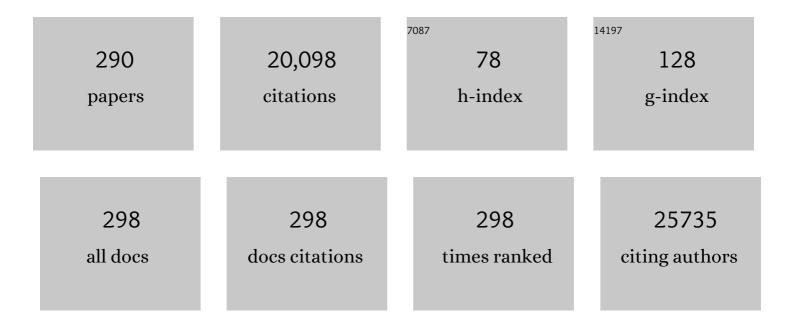
Wenjun Zhang

List of Publications by Year in descending order

Source: https://exaly.com/author-pdf/3911702/publications.pdf Version: 2024-02-01



WENILIN ZHANC

#	Article	IF	CITATIONS
1	A graphene quantum dot photodynamic therapy agent with high singlet oxygen generation. Nature Communications, 2014, 5, 4596.	5.8	1,141
2	Photosensitizers for Photodynamic Therapy. Advanced Healthcare Materials, 2019, 8, e1900132.	3.9	637
3	Green Synthesis of Bifunctional Fluorescent Carbon Dots from Garlic for Cellular Imaging and Free Radical Scavenging. ACS Applied Materials & Interfaces, 2015, 7, 17054-17060.	4.0	494
4	Silicon nanowires for rechargeable lithium-ion battery anodes. Applied Physics Letters, 2008, 93, .	1.5	372
5	Hierarchical nanotubes assembled from MoS 2 -carbon monolayer sandwiched superstructure nanosheets for high-performance sodium ion batteries. Nano Energy, 2016, 22, 27-37.	8.2	333
6	Oxygen Vacancy Engineering Promoted Photocatalytic Ammonia Synthesis on Ultrathin Two-Dimensional Bismuth Oxybromide Nanosheets. Nano Letters, 2018, 18, 7372-7377.	4.5	308
7	Interlayer Nanoarchitectonics of Twoâ€Dimensional Transitionâ€Metal Dichalcogenides Nanosheets for Energy Storage and Conversion Applications. Advanced Energy Materials, 2017, 7, 1700571.	10.2	303
8	Review on photocatalytic and electrocatalytic artificial nitrogen fixation for ammonia synthesis at mild conditions: Advances, challenges and perspectives. Nano Research, 2019, 12, 1229-1249.	5.8	301
9	One-dimensional II–VI nanostructures: Synthesis, properties and optoelectronic applications. Nano Today, 2010, 5, 313-336.	6.2	293
10	Vertically Aligned Boron Nitride Nanosheets: Chemical Vapor Synthesis, Ultraviolet Light Emission, and Superhydrophobicity. ACS Nano, 2010, 4, 414-422.	7.3	291
11	Oxygenâ€Incorporated NiMoP Nanotube Arrays as Efficient Bifunctional Electrocatalysts For Ureaâ€Assisted Energyâ€Saving Hydrogen Production in Alkaline Electrolyte. Advanced Functional Materials, 2021, 31, 2104951.	7.8	247
12	Two-photon-excited near-infrared emissive carbon dots as multifunctional agents for fluorescence imaging and photothermal therapy. Nano Research, 2017, 10, 3113-3123.	5.8	246
13	An Aqueous Znâ€ion Hybrid Supercapacitor with High Energy Density and Ultrastability up to 80 000 Cycles. Advanced Energy Materials, 2019, 9, 1902915.	10.2	244
14	Iron Vacancies Induced Bifunctionality in Ultrathin Feroxyhyte Nanosheets for Overall Water Splitting. Advanced Materials, 2018, 30, e1803144.	11.1	225
15	Strong Capillarity, Chemisorption, and Electrocatalytic Capability of Crisscrossed Nanostraws Enabled Flexible, High-Rate, and Long-Cycling Lithium–Sulfur Batteries. ACS Nano, 2018, 12, 4868-4876.	7.3	222
16	Lithiophilic Cu uOâ€Ni Hybrid Structure: Advanced Current Collectors Toward Stable Lithium Metal Anodes. Advanced Materials, 2018, 30, 1705830.	11.1	217
17	Hierarchical Composite Electrodes of Nickel Oxide Nanoflake 3D Graphene for Highâ€Performance Pseudocapacitors. Advanced Functional Materials, 2014, 24, 6372-6380.	7.8	210
18	Ultralarge elastic deformation of nanoscale diamond. Science, 2018, 360, 300-302.	6.0	208

#	Article	IF	CITATIONS
19	Porous-Shell Vanadium Nitride Nanobubbles with Ultrahigh Areal Sulfur Loading for High-Capacity and Long-Life Lithium–Sulfur Batteries. Nano Letters, 2017, 17, 7839-7846.	4.5	206
20	Hierarchical composite structure of few-layers MoS 2 nanosheets supported by vertical graphene on carbon cloth for high-performance hydrogen evolution reaction. Nano Energy, 2015, 18, 196-204.	8.2	191
21	Biocompatible D–A Semiconducting Polymer Nanoparticle with Lightâ€Harvesting Unit for Highly Effective Photoacoustic Imaging Guided Photothermal Therapy. Advanced Functional Materials, 2017, 27, 1605094.	7.8	188
22	Arrays of ZnO/Zn _{<i>x</i>} Cd _{1–<i>x</i>} Se Nanocables: Band Gap Engineering and Photovoltaic Applications. Nano Letters, 2011, 11, 4138-4143.	4.5	185
23	High Detectivity Solarâ€Blind Highâ€Temperature Deepâ€Ultraviolet Photodetector Based on Multiâ€Layered (<i>l</i> 00) Facetâ€Oriented <i>β</i> â€Ga ₂ O ₃ Nanobelts. Small, 2014, 10, 1848-185	6. ^{5.2}	185
24	Surfaceâ€Dominated Transport Properties of Silicon Nanowires. Advanced Functional Materials, 2008, 18, 3251-3257.	7.8	180
25	Unconventional Nickel Nitride Enriched with Nitrogen Vacancies as a Highâ€Efficiency Electrocatalyst for Hydrogen Evolution. Advanced Science, 2018, 5, 1800406.	5.6	163
26	Three-dimensional-networked NiCo2S4 nanosheet array/carbon cloth anodes for high-performance lithium-ion batteries. NPG Asia Materials, 2015, 7, e195-e195.	3.8	158
27	In situ incorporation of FeS nanoparticles/carbon nanosheets composite with an interconnected porous structure as a high-performance anode for lithium ion batteries. Journal of Materials Chemistry A, 2016, 4, 3697-3703.	5.2	153
28	Grapheneâ€Nanowallâ€Decorated Carbon Felt with Excellent Electrochemical Activity Toward VO ₂ ⁺ /VO ²⁺ Couple for All Vanadium Redox Flow Battery. Advanced Science, 2016, 3, 1500276.	5.6	152
29	Surface Engineering of ZnO Nanostructures for Semiconductor‧ensitized Solar Cells. Advanced Materials, 2014, 26, 5337-5367.	11.1	149
30	Photothermal Theragnosis Synergistic Therapy Based on Bimetal Sulphide Nanocrystals Rather Than Nanocomposites. Advanced Materials, 2015, 27, 1339-1345.	11.1	149
31	Self-Monitoring and Self-Delivery of Photosensitizer-Doped Nanoparticles for Highly Effective Combination Cancer Therapy <i>in Vitro</i> and <i>in Vivo</i> . ACS Nano, 2015, 9, 9741-9756.	7.3	149
32	Light-emitting diodes enhanced by localized surface plasmon resonance. Nanoscale Research Letters, 2011, 6, 199.	3.1	147
33	Carbon Nanoparticle-based Ratiometric Fluorescent Sensor for Detecting Mercury Ions in Aqueous Media and Living Cells. ACS Applied Materials & Interfaces, 2014, 6, 21270-21278.	4.0	144
34	Three-dimensional Sn–graphene anode for high-performance lithium-ion batteries. Nanoscale, 2013, 5, 10599.	2.8	141
35	Germanium–graphene composite anode for high-energy lithium batteries with long cycle life. Journal of Materials Chemistry A, 2013, 1, 1821-1826.	5.2	138
36	Highly Efficient Electrochemical Reduction of Nitrogen to Ammonia on Surface Termination Modified Ti ₃ C ₂ T _{<i>x</i>} MXene Nanosheets. ACS Nano, 2020, 14, 9089-9097.	7.3	137

#	Article	IF	CITATIONS
37	rGO/SnS ₂ /TiO ₂ heterostructured composite with dual-confinement for enhanced lithium-ion storage. Journal of Materials Chemistry A, 2017, 5, 25056-25063.	5.2	136
38	Copper substituted P2-type Na _{0.67} Cu _x Mn _{1â^'x} O ₂ : a stable high-power sodium-ion battery cathode. Journal of Materials Chemistry A, 2015, 3, 22846-22852.	5.2	135
39	Iron(<scp>ii</scp>) molybdate (FeMoO ₄) nanorods as a high-performance anode for lithium ion batteries: structural and chemical evolution upon cycling. Journal of Materials Chemistry A, 2015, 3, 20527-20534.	5.2	135
40	Core–Shell Si/C Nanospheres Embedded in Bubble Sheetâ€like Carbon Film with Enhanced Performance as Lithium Ion Battery Anodes. Small, 2015, 11, 1345-1351.	5.2	131
41	High-Rate Deposition of High-Quality, Thick Cubic Boron Nitride Films by Bias-Assisted DC Jet Plasma Chemical Vapor Deposition. Japanese Journal of Applied Physics, 2000, 39, L442-L444.	0.8	130
42	Solventâ€Polarityâ€Engineered Controllable Synthesis of Highly Fluorescent Cesium Lead Halide Perovskite Quantum Dots and Their Use in White Lightâ€Emitting Diodes. Advanced Functional Materials, 2016, 26, 8478-8486.	7.8	129
43	Vertically Aligned Graphene Nanosheet Arrays: Synthesis, Properties and Applications in Electrochemical Energy Conversion and Storage. Advanced Energy Materials, 2017, 7, 1700678.	10.2	126
44	Surface passivation and band engineering: a way toward high efficiency graphene–planar Si solar cells. Journal of Materials Chemistry A, 2013, 1, 8567.	5.2	123
45	High-efficiency graphene/Si nanoarray Schottky junction solar cells via surface modification and graphene doping. Journal of Materials Chemistry A, 2013, 1, 6593.	5.2	122
46	Copolythiophene-Derived Colorimetric and Fluorometric Sensor for Visually Supersensitive Determination of Lipopolysaccharide. Journal of the American Chemical Society, 2012, 134, 6685-6694.	6.6	115
47	Bactericidal activity of biomimetic diamond nanocone surfaces. Biointerphases, 2016, 11, 011014.	0.6	115
48	In situnitrogen-doped graphene grown from polydimethylsiloxane by plasma enhanced chemical vapor deposition. Nanoscale, 2013, 5, 600-605.	2.8	114
49	Sulfur-deficient MoS ₂ grown inside hollow mesoporous carbon as a functional polysulfide mediator. Journal of Materials Chemistry A, 2019, 7, 12068-12074.	5.2	112
50	Layer-stacked cobalt ferrite (CoFe ₂ O ₄) mesoporous platelets for high-performance lithium ion battery anodes. Journal of Materials Chemistry A, 2015, 3, 6990-6997.	5.2	111
51	Editable asymmetric all-solid-state supercapacitors based on high-strength, flexible, and programmable 2D-metal–organic framework/reduced graphene oxide self-assembled papers. Journal of Materials Chemistry A, 2018, 6, 20254-20266.	5.2	110
52	Diamond nanostructures for drug delivery, bioimaging, and biosensing. Chemical Society Reviews, 2017, 46, 734-760.	18.7	109
53	Oxygen-deficient titanium dioxide as a functional host for lithium–sulfur batteries. Journal of Materials Chemistry A, 2019, 7, 10346-10353.	5.2	109
54	Photoconductivity of a Single Smallâ€Molecule Organic Nanowire. Advanced Materials, 2008, 20, 2427-2432.	11.1	108

#	Article	IF	CITATIONS
55	Layered double hydroxide nanostructures and nanocomposites for biomedical applications. Journal of Materials Chemistry B, 2019, 7, 5583-5601.	2.9	108
56	Poking cells for efficient vector-free intracellular delivery. Nature Communications, 2014, 5, 4466.	5.8	104
57	In Situ Carbon-Doped Mo(Se _{0.85} S _{0.15}) ₂ Hierarchical Nanotubes as Stable Anodes for High-Performance Sodium-Ion Batteries. Small, 2015, 11, 5667-5674.	5.2	101
58	Visible–NIR photodetectors based on CdTe nanoribbons. Nanoscale, 2012, 4, 2914.	2.8	99
59	MoS2 nanobelts with (002) plane edges-enriched flat surfaces for high-rate sodium and lithium storage. Energy Storage Materials, 2018, 15, 65-74.	9.5	96
60	Graphitic carbon nitride solid nanofilms for selective and recyclable sensing of Cu ²⁺ and Ag ⁺ in water and serum. Chemical Communications, 2014, 50, 15415-15418.	2.2	95
61	Nanocapillarity and Nanoconfinement Effects of Pipet-like Bismuth@Carbon Nanotubes for Highly Efficient Electrocatalytic CO ₂ Reduction. Nano Letters, 2021, 21, 2650-2657.	4.5	95
62	A carbon dot-based fluorescence turn-on sensor for hydrogen peroxide with a photo-induced electron transfer mechanism. Chemical Communications, 2015, 51, 15574-15577.	2.2	94
63	Three-dimensional networked NiCo ₂ O ₄ /MnO ₂ branched nanowire heterostructure arrays on nickel foam with enhanced supercapacitor performance. Journal of Materials Chemistry A, 2015, 3, 1717-1723.	5.2	94
64	Controlled Assembly of Highly Ramanâ€Enhancing Silver Nanocap Arrays Templated by Porous Anodic Alumina Membranes. Small, 2009, 5, 2333-2337.	5.2	92
65	Recent developments of wide-bandgap semiconductor based UV sensors. Diamond and Related Materials, 2009, 18, 860-864.	1.8	92
66	Lysosome-targetable carbon dots for highly efficient photothermal/photodynamic synergistic cancer therapy and photoacoustic/two-photon excited fluorescence imaging. Chemical Engineering Journal, 2020, 388, 124212.	6.6	92
67	Highly efficient microwave absorption properties and broadened absorption bandwidth of MoS2-iron oxide hybrids and MoS2-based reduced graphene oxide hybrids with Hetero-structures. Applied Surface Science, 2018, 462, 872-882.	3.1	90
68	A three-dimensional graphene scaffold supported thin film silicon anode for lithium-ion batteries. Journal of Materials Chemistry A, 2013, 1, 10092.	5.2	88
69	Surfaceâ€Engineered Black Niobium Oxide@Graphene Nanosheets for Highâ€Performance Sodiumâ€IPotassiumâ€Ion Full Batteries. Small, 2019, 15, e1901272.	5.2	88
70	Nitrogen-Doped Carbon Nanotube Forests Planted on Cobalt Nanoflowers as Polysulfide Mediator for Ultralow Self-Discharge and High Areal-Capacity Lithium–Sulfur Batteries. Nano Letters, 2018, 18, 7949-7954.	4.5	85
71	Vertical nanostructure arrays by plasma etching for applications in biology, energy, and electronics. Nano Today, 2013, 8, 265-289.	6.2	84
72	Silicon nanowire sensors for Hg2+ and Cd2+ ions. Applied Physics Letters, 2009, 94, .	1.5	83

#	Article	IF	CITATIONS
73	Synthesis of Honeycombâ€like Mesoporous Pyrite FeS ₂ Microspheres as Efficient Counter Electrode in Quantum Dots Sensitized Solar Cells. Small, 2014, 10, 4754-4759.	5.2	83
74	Fe _{1â^'x} S/C nanocomposites from sugarcane waste-derived microporous carbon for high-performance lithium ion batteries. Green Chemistry, 2016, 18, 3029-3039.	4.6	83
75	Superior Pseudocapacitive Lithium-Ion Storage in Porous Vanadium Oxides@C Heterostructure Composite. ACS Applied Materials & Interfaces, 2017, 9, 43665-43673.	4.0	83
76	A Biocompatible Free Radical Nanogenerator with Realâ€īme Monitoring Capability for High Performance Sequential Hypoxic Tumor Therapy. Advanced Functional Materials, 2019, 29, 1903436.	7.8	83
77	Highly sensitive fluorescent probe for thiols based on combination of PET and ESIPT mechanisms. Sensors and Actuators B: Chemical, 2011, 156, 332-337.	4.0	82
78	Dendritic Heterojunction Nanowire Arrays for High-Performance Supercapacitors. Scientific Reports, 2015, 5, 7862.	1.6	82
79	Superhydrophobic SERS chip based on a Ag coated natural taro-leaf. Nanoscale, 2016, 8, 11487-11493.	2.8	82
80	An oxygen-deficient vanadium oxide@N-doped carbon heterostructure for sodium-ion batteries: insights into the charge storage mechanism and enhanced reaction kinetics. Journal of Materials Chemistry A, 2020, 8, 3450-3458.	5.2	81
81	A recyclable carbon nanoparticle-based fluorescent probe for highly selective and sensitive detection of mercapto biomolecules. Journal of Materials Chemistry B, 2015, 3, 127-134.	2.9	79
82	Heterointerface engineering of trilayer-shelled ultrathin MoS ₂ /MoP/N-doped carbon hollow nanobubbles for efficient hydrogen evolution. Journal of Materials Chemistry A, 2018, 6, 24783-24792.	5.2	79
83	Degradable Hollow Mesoporous Silicon/Carbon Nanoparticles for Photoacoustic Imaging-Guided Highly Effective Chemo-Thermal Tumor Therapy <i>in Vitro</i> and <i>in Vivo</i> . Theranostics, 2017, 7, 3007-3020.	4.6	78
84	Recent progress in organic molecule/graphene interfaces. Nano Today, 2013, 8, 388-402.	6.2	77
85	P2-Type Na _{<i>x</i>} Cu _{0.15} Ni _{0.20} Mn _{0.65} O ₂ Cathodes with High Voltage for High-Power and Long-Life Sodium-Ion Batteries. ACS Applied Materials & Interfaces, 2016, 8, 31661-31668.	4.0	77
86	High-performance microwave absorption materials based on MoS 2 -graphene isomorphic hetero-structures. Journal of Alloys and Compounds, 2018, 758, 62-71.	2.8	77
87	Carbon Dots as Multifunctional Phototheranostic Agents for Photoacoustic/Fluorescence Imaging and Photothermal/Photodynamic Synergistic Cancer Therapy. Advanced Therapeutics, 2018, 1, 1800077.	1.6	77
88	Visualizing the Initial Step of Self-Assembly and the Phase Transition by Stereogenic Amphiphiles with Aggregation-Induced Emission. ACS Nano, 2019, 13, 839-846.	7.3	77
89	Facile synthesis and electrochemical characterization of porous and dense TiO2 nanospheres for lithium-ion battery applications. Journal of Power Sources, 2011, 196, 6394-6399.	4.0	75
90	Light-weight 3D Co–N-doped hollow carbon spheres as efficient electrocatalysts for rechargeable zinc–air batteries. Nanoscale, 2018, 10, 10412-10419.	2.8	73

#	Article	IF	CITATIONS
91	A silicon nanowire–reduced graphene oxide composite as a high-performance lithium ion battery anode material. Nanoscale, 2014, 6, 3353.	2.8	71
92	Achieving highly efficient pH-universal hydrogen evolution by superhydrophilic amorphous/crystalline Rh(OH)3/NiTe coaxial nanorod array electrode. Applied Catalysis B: Environmental, 2022, 305, 121088.	10.8	71
93	Ni single atoms anchored on N-doped carbon nanosheets as bifunctional electrocatalysts for Urea-assisted rechargeable Zn-air batteries. Applied Catalysis B: Environmental, 2022, 310, 121352.	10.8	71
94	Template-Directed Bifunctional Dodecahedral CoP/CN@MoS ₂ Electrocatalyst for High Efficient Water Splitting. ACS Applied Materials & Interfaces, 2019, 11, 36649-36657.	4.0	70
95	Size Controllable and Surface Tunable Zeolitic Imidazolate Framework-8–Poly(acrylic acid sodium) Tj ETQq1 1 ACS Applied Materials & Interfaces, 2017, 9, 32990-33000.	0.784314 4.0	rgBT /Over 69
96	Flexible Diamond Fibers for Highâ€Energyâ€Đensity Zincâ€Ion Supercapacitors. Advanced Energy Materials, 2020, 10, 2002202.	10.2	69
97	Advanced Materials and Nanotechnology for Drug Delivery. Advanced Materials, 2014, 26, 5533-5540.	11.1	66
98	Mesoporous Nanosheet Networked Hybrids of Cobalt Oxide and Cobalt Phosphate for Efficient Electrochemical and Photoelectrochemical Oxygen Evolution. Small, 2017, 13, 1701875.	5.2	66
99	The introducing of fluorine into the deposition of BN: a successful method to obtain high-quality, thick cBN films with low residual stress. Diamond and Related Materials, 2001, 10, 1868-1874.	1.8	65
100	CdS/CdSe Double-Sensitized ZnO Nanocable Arrays Synthesized by Chemical Solution Method and Their Photovoltaic Applications. Journal of Physical Chemistry C, 2012, 116, 2656-2661.	1.5	65
101	Influence of Ti content on the structure and tribological properties of Ti-DLC coatings in water lubrication. Diamond and Related Materials, 2012, 25, 163-175.	1.8	64
102	Engineering the coordination environment enables molybdenum single-atom catalyst for efficient oxygen reduction reaction. Journal of Catalysis, 2020, 389, 150-156.	3.1	64
103	Recent Advances in Cubic Boron Nitride Deposition. MRS Bulletin, 2003, 28, 184-188.	1.7	63
104	<i>In situ</i> nitridated porous nanosheet networked Co ₃ O ₄ –Co ₄ N heteronanostructures supported on hydrophilic carbon cloth for highly efficient electrochemical hydrogen evolution. Journal of Materials Chemistry A, 2019, 7, 775-782.	5.2	63
105	Facile solution growth of vertically aligned ZnO nanorods sensitized with aqueous CdS and CdSe quantum dots for photovoltaic applications. Nanoscale Research Letters, 2011, 6, 340.	3.1	61
106	Microstructure and water-lubricated friction and wear properties of CrN(C) coatings with different carbon contents. Applied Surface Science, 2013, 268, 579-587.	3.1	61
107	<i>In situ</i> formation of NaTi ₂ (PO ₄) ₃ cubes on Ti ₃ C ₂ MXene for dual-mode sodium storage. Journal of Materials Chemistry A, 2018, 6, 18525-18532.	5.2	60
108	Low-cost porous Cu2ZnSnSe4 film remarkably superior to noble Pt as counter electrode in quantum dot-sensitized solar cell system. Journal of Power Sources, 2013, 226, 359-362.	4.0	57

#	Article	IF	CITATIONS
109	Graphene encapsulated and SiC reinforced silicon nanowires as an anode material for lithium ion batteries. Nanoscale, 2013, 5, 8689.	2.8	56
110	Self-Assembly of Electron Donor–Acceptor-Based Carbazole Derivatives: Novel Fluorescent Organic Nanoprobes for Both One- and Two-Photon Cellular Imaging. ACS Applied Materials & Interfaces, 2016, 8, 11355-11365.	4.0	56
111	Electrochemical Energy Storage Application and Degradation Analysis of Carbon-Coated Hierarchical NiCo2S4 Core-Shell Nanowire Arrays Grown Directly on Graphene/Nickel Foam. Scientific Reports, 2016, 6, 20264.	1.6	56
112	Biodegradable Natural Product-Based Nanoparticles for Near-Infrared Fluorescence Imaging-Guided Sonodynamic Therapy. ACS Applied Materials & Interfaces, 2019, 11, 18178-18185.	4.0	55
113	Surface plasmon resonance enhanced direct Z-scheme TiO ₂ /ZnTe/Au nanocorncob heterojunctions for efficient photocatalytic overall water splitting. Nanoscale, 2019, 11, 9053-9060.	2.8	55
114	Nanostructured and Boron-Doped Diamond as an Electrocatalyst for Nitrogen Fixation. ACS Energy Letters, 2020, 5, 2590-2596.	8.8	55
115	A highly selective fluorescent sensor for fluoride in aqueous solution based on the inhibition of excited-state intramolecular proton transfer. Sensors and Actuators B: Chemical, 2010, 146, 260-265.	4.0	54
116	Spray deposition of water-soluble multiwall carbon nanotube and Cu2ZnSnSe4 nanoparticle composites as highly efficient counter electrodes in a quantum dot-sensitized solar cell system. Nanoscale, 2013, 5, 6992.	2.8	54
117	Near-Infrared Light-Triggered Lysosome-Targetable Carbon Dots for Photothermal Therapy of Cancer. ACS Applied Materials & Interfaces, 2021, 13, 53610-53617.	4.0	54
118	Hot spots in highly Raman-enhancing silver nano-dendrites. Journal Physics D: Applied Physics, 2009, 42, 175403.	1.3	53
119	Bismuth nanorod networks confined in a robust carbon matrix as long-cycling and high-rate potassium-ion battery anodes. Journal of Materials Chemistry A, 2020, 8, 8440-8446.	5.2	52
120	Metal organic frameworks for antibacterial applications. Chemical Engineering Journal, 2022, 435, 134975.	6.6	52
121	The roles of hydrogen and fluorine in the deposition of cubic boron nitride films in the Ar–N2–BF3–H2 system. Chemical Physics Letters, 2000, 330, 243-248.	1.2	51
122	A novel fluorogenic hybrid material for selective sensing of thiophenols. Journal of Materials Chemistry, 2011, 21, 13561.	6.7	51
123	Highly efficient overall water splitting driven by all-inorganic perovskite solar cells and promoted by bifunctional bimetallic phosphide nanowire arrays. Journal of Materials Chemistry A, 2018, 6, 20076-20082.	5.2	51
124	Pyrene-derivatized highly fluorescent carbon dots for the sensitive and selective determination of ferric ions and dopamine. Dyes and Pigments, 2019, 170, 107574.	2.0	51
125	Facile synthesis of laminate-structured graphene sheet–Fe3O4 nanocomposites with superior high reversible specific capacity and cyclic stability for lithium-ion batteries. RSC Advances, 2012, 2, 10680.	1.7	50
126	Nitrogenâ€Doped Grapheneâ€Encapsulated Nickel–Copper Alloy Nanoflower for Highly Efficient Electrochemical Hydrogen Evolution Reaction. Small, 2019, 15, e1901545.	5.2	50

#	Article	IF	CITATIONS
127	Highly stable organic fluorescent nanorods for living-cell imaging. Nano Research, 2015, 8, 2380-2389.	5.8	49
128	Water-Soluble Polythiophene for Two-Photon Excitation Fluorescence Imaging and Photodynamic Therapy of Cancer. ACS Applied Materials & Interfaces, 2017, 9, 14590-14595.	4.0	49
129	Nanoparticles Encapsulated in Porous Carbon Matrix Coated on Carbon Fibers: An Ultrastable Cathode for Liâ€ion Batteries. Advanced Energy Materials, 2017, 7, 1601363.	10.2	48
130	The effects of dc bias voltage on the crystal size and crystal quality. of cBN films. Applied Physics A: Materials Science and Processing, 2000, 71, 469-472.	1.1	47
131	Electronic structure of MoO3â^x/graphene interface. Carbon, 2013, 65, 46-52.	5.4	47
132	Optically tunable fluorescent carbon nanoparticles and their application in fluorometric sensing of copper ions. Nano Research, 2019, 12, 2576-2583.	5.8	47
133	Phase Conversion from Hexagonal CuS _{<i>y</i>} Se _{1–<i>y</i>} to Cubic Cu _{2–<i>x</i>} S _{<i>y</i>} Se _{1–<i>y</i>} : Composition Variation, Morphology Evolution, Optical Tuning, and Solar Cell Applications. ACS Applied Materials & amp; Interfaces, 2014, 6, 16352-16359.	4.0	46
134	Cubic boron nitride films for industrial applications. Diamond and Related Materials, 2005, 14, 1784-1790.	1.8	45
135	Violet-blue LEDs based on p-GaN/n-ZnO nanorods and their stability. Nanotechnology, 2011, 22, 245202.	1.3	43
136	Plasmonic nanopillar array embedded microfluidic chips: an in situ SERS monitoring platform. Journal of Materials Chemistry A, 2015, 3, 6408-6413.	5.2	43
137	A Novel Type of Aqueous Dispersible Ultrathin-Layered Double Hydroxide Nanosheets for in Vivo Bioimaging and Drug Delivery. ACS Applied Materials & Interfaces, 2017, 9, 34185-34193.	4.0	42
138	Heteroepitaxial nucleation of diamond on Si(100) via double bias-assisted hot filament chemical vapor deposition. Diamond and Related Materials, 2000, 9, 134-139.	1.8	41
139	Deposition of thick cubic boron nitride films: The route to practical applications. Diamond and Related Materials, 2005, 14, 1154-1162.	1.8	41
140	van der Waals Epitaxial Growth and Interfacial Passivation of Two-Dimensional Single-Crystalline Few-Layer Gray Arsenic Nanoflakes. Chemistry of Materials, 2019, 31, 4524-4535.	3.2	41
141	Defect engineering of nanostructured electrocatalysts for enhancing nitrogen reduction. Journal of Materials Chemistry A, 2020, 8, 7457-7473.	5.2	41
142	Nitrogen-Doped Carbon-Encapsulated Antimony Sulfide Nanowires Enable High Rate Capability and Cyclic Stability for Sodium-Ion Batteries. ACS Applied Nano Materials, 2019, 2, 1457-1465.	2.4	40
143	Copolythiophene-Derived Colorimetric and Fluorometric Sensor for Lysophosphatidic Acid Based on Multipoint Interactions. ACS Applied Materials & Interfaces, 2013, 5, 2283-2288.	4.0	39
144	Optofluidic detection for cellular phenotyping. Lab on A Chip, 2012, 12, 3552.	3.1	38

#	Article	IF	CITATIONS
145	A Diamond Nanoneedle Array for Potential Highâ€Throughput Intracellular Delivery. Advanced Healthcare Materials, 2013, 2, 1103-1107.	3.9	38
146	MoS ₂ Nanosheets Supported on Hollow Carbon Spheres as Efficient Catalysts for Electrochemical Hydrogen Evolution Reaction. ACS Omega, 2017, 2, 5087-5094.	1.6	38
147	Construction of MoO ₂ Quantum Dot–Graphene and MoS ₂ Nanoparticle–Graphene Nanoarchitectures toward Ultrahigh Lithium Storage Capability. ACS Applied Materials & Interfaces, 2017, 9, 28441-28450.	4.0	38
148	Three-dimensional spongy framework as superlyophilic, strongly absorbing, and electrocatalytic polysulfide reservoir layer for high-rate and long-cycling lithium-sulfur batteries. Nano Research, 2018, 11, 6436-6446.	5.8	38
149	Defect-engineered vanadium trioxide nanofiber bundle@graphene hybrids for high-performance all-vanadate Na-ion and K-ion full batteries. Journal of Materials Chemistry A, 2019, 7, 19581-19588.	5.2	38
150	Dual Fenton Catalytic Nanoreactor for Integrative Type-I and Type-II Photodynamic Therapy Against Hypoxic Cancer Cells. ACS Applied Bio Materials, 2019, 2, 3854-3860.	2.3	38
151	Deposition of large-area, high-quality cubic boron nitride films by ECR-enhanced microwave-plasma CVD. Applied Physics A: Materials Science and Processing, 2003, 76, 953-955.	1.1	37
152	Effect of titanium or chromium content on the electrochemical properties of amorphous carbon coatings in simulated body fluid. Electrochimica Acta, 2013, 112, 603-611.	2.6	37
153	Green Mass Production of Pure Nanodrugs via an Ice-Template-Assisted Strategy. Nano Letters, 2019, 19, 658-665.	4.5	37
154	Fluorinated Carbonate Electrolyte with Superior Oxidative Stability Enables Longâ€Term Cycle Stability of Na _{2/3} Ni _{1/3} Mn _{2/3} O ₂ Cathodes in Sodiumâ€Ion Batteries. Advanced Energy Materials, 2021, 11, 2002737.	10.2	37
155	High-Sensitivity and Stable Cellular Fluorescence Imaging by Patterned Silver Nanocap Arrays. ACS Applied Materials & Interfaces, 2010, 2, 2465-2470.	4.0	36
156	"Seeing―and Controlling Photoisomerization by (<i>Z</i>)-/(<i>E</i>)-Isomers with Aggregation-Induced Emission Characteristics. ACS Nano, 2019, 13, 12120-12126.	7.3	36
157	Boosting Polysulfide Conversion in Lithium–Sulfur Batteries by Cobalt-Doped Vanadium Nitride Microflowers. ACS Applied Energy Materials, 2020, 3, 4523-4530.	2.5	36
158	A nanoindentation study of thick cBN films prepared by chemical vapor deposition. Journal of Crystal Growth, 2003, 247, 438-444.	0.7	35
159	Interrogation of Cellular Innate Immunity by Diamond-Nanoneedle-Assisted Intracellular Molecular Fishing. Nano Letters, 2015, 15, 7058-7063.	4.5	35
160	A graphene rheostat for highly durable and stretchable strain sensor. InformaÄnÃ-Materiály, 2019, 1, 396-406.	8.5	35
161	Structure analysis of cBN films prepared by DC jet plasma CVD from an Ar–N2–BF3–H2 gas system. Diamond and Related Materials, 2001, 10, 1881-1885.	1.8	34
162	Fabrication of diamond nanocones and nanowhiskers by bias-assisted plasma etching. Diamond and Related Materials, 2007, 16, 1208-1212.	1.8	34

#	Article	IF	CITATIONS
163	Recyclable Nonâ€Enzymatic Glucose Sensor Based on Ni/NiTiO ₃ /TiO ₂ Nanotube Arrays. ChemPlusChem, 2015, 80, 576-582.	1.3	34
164	Water Evaporation Induced Conversion of CuSe Nanoflakes to Cu _{2â^'<i>x</i>} Se Hierarchical Columnar Superstructures for High-Performance Solar Cell Applications. Particle and Particle Systems Characterization, 2015, 32, 840-847.	1.2	34
165	Lithiophilicity conversion of the Cu surface through facile thermal oxidation: boosting a stable Li–Cu composite anode through melt infusion. Journal of Materials Chemistry A, 2019, 7, 5726-5732.	5.2	34
166	Electrochemically Stable Sodium Metalâ€Tellurium/Carbon Nanorods Batteries. Advanced Energy Materials, 2019, 9, 1903046.	10.2	33
167	Electrochemical Capacitors with Confined Redox Electrolytes and Porous Electrodes. Advanced Materials, 2022, 34, e2202380.	11.1	33
168	Synthesis of SiC decorated carbonaceous nanorods and its hierarchical composites Si@SiC@C for high-performance lithium ion batteries. Journal of Alloys and Compounds, 2015, 646, 966-972.	2.8	32
169	Selfâ€Adaptive Electrode with SWCNT Bundles as Elastic Substrate for Highâ€Rate and Longâ€Cycleâ€Life Lithium/Sodium Ion Batteries. Small, 2018, 14, e1802913.	5.2	32
170	UV-to-IR highly transparent ultrathin diamond nanofilms with intriguing performances: Anti-fogging, self-cleaning and self-lubricating. Applied Surface Science, 2020, 527, 146733.	3.1	32
171	Structuring single- and nano-crystalline diamond cones. Diamond and Related Materials, 2004, 13, 1037-1043.	1.8	31
172	Stability of submicron AlGaN/GaN HEMT devices irradiated by gamma rays. Microelectronic Engineering, 2009, 86, 37-40.	1.1	31
173	Influence of carbon content on the microstructure and tribological properties of TiN(C) coatings in water lubrication. Surface and Coatings Technology, 2012, 206, 3777-3787.	2.2	31
174	Laser Processing of Flexible In-Plane Micro-supercapacitors: Progresses in Advanced Manufacturing of Nanostructured Electrodes. ACS Nano, 2022, 16, 10088-10129.	7.3	31
175	Corrosion resistance of ZrO ₂ –Zr-coated biodegradable surgical magnesium alloy. Journal of Materials Research, 2008, 23, 312-319.	1.2	30
176	Synthesis and characterization of hard ternary AlMgB composite films prepared by sputter deposition. Thin Solid Films, 2010, 518, 5372-5377.	0.8	30
177	Controlled Surface Chemistry of Diamond/β-SiC Composite Films for Preferential Protein Adsorption. Langmuir, 2014, 30, 1089-1099.	1.6	30
178	Single zinc-doped indium oxide nanowire as driving transistor for organic light-emitting diode. Applied Physics Letters, 2008, 92, .	1.5	29
179	Molecular Structure and Chemical Property of a Divalent Metallofullerene Yb@ <i>C</i> ₂ (13)-C ₈₄ . Journal of the American Chemical Society, 2013, 135, 12730-12735.	6.6	29
180	Firmly anchored photosensitizer Chlorin e6 to layered double hydroxide nanoflakes for highly efficient photodynamic therapy in vivo. Chemical Communications, 2017, 53, 2339-2342.	2.2	29

#	Article	IF	CITATIONS
181	Single-Atom Metal Anchored Zr ₆ -Cluster-Porphyrin Framework Hollow Nanocapsules with Ultrahigh Active-Center Density for Electrocatalytic CO ₂ Reduction. Nano Letters, 2022, 22, 3340-3348.	4.5	29
182	Tunable Silver Nanocap Superlattice Arrays for Surface-Enhanced Raman Scattering. Journal of Physical Chemistry C, 2011, 115, 24328-24333.	1.5	28
183	Dilute Aqueousâ€Aprotic Hybrid Electrolyte Enabling a Wide Electrochemical Window through Solvation Structure Engineering. Advanced Materials, 2021, 33, e2102390.	11.1	28
184	Recent developments in optofluidic-surface-enhanced Raman scattering systems: Design, assembly, and advantages. Journal of Materials Research, 2011, 26, 170-185.	1.2	27
185	Diamondâ€Nanoneedleâ€Arrayâ€Facilitated Intracellular Delivery and the Potential Influence on Cell Physiology. Advanced Healthcare Materials, 2016, 5, 1157-1168.	3.9	27
186	Element-doped graphitic carbon nitride: confirmation of doped elements and applications. Nanoscale Advances, 2021, 3, 4370-4387.	2.2	27
187	Tailoring light emission properties of organic emitter by coupling to resonance-tuned silver nanoantenna arrays. Applied Physics Letters, 2009, 95, .	1.5	26
188	Studying cubic boron nitride by Raman and infrared spectroscopies. Diamond and Related Materials, 2010, 19, 968-971.	1.8	26
189	Boosting oxygen evolution reaction on graphene through engineering electronic structure. Carbon, 2020, 170, 414-420.	5.4	26
190	Tunable Photoâ€Electrochemistry of Patterned TiO ₂ /BDD Heterojunctions. Small Methods, 2020, 4, 2000257.	4.6	26
191	Synthesis of Cu3BiS3 and AgBiS2 crystallites with controlled morphology using hypocrellin template and their catalytic role in the polymerization of alkylsilane. Journal of Materials Science, 2012, 47, 4159-4166.	1.7	25
192	Synthesis of Mesoporous ZIFâ€8 Nanoribbons and their Conversion into Carbon Nanoribbons for Highâ€Performance Supercapacitors. Chemistry - A European Journal, 2018, 24, 11185-11192.	1.7	24
193	Microstructure and tribological properties of cubic boron nitride films on Si 3 N 4 inserts via boron-doped diamond buffer layers. Diamond and Related Materials, 2014, 49, 9-13.	1.8	23
194	The growth of thick cBN films employing fluorine chemistry and ECR deposition. Diamond and Related Materials, 2003, 12, 1162-1168.	1.8	22
195	Structure and water-lubricated tribological properties of Cr/a-C coatings with different Cr contents. Tribology International, 2013, 67, 104-115.	3.0	22
196	Fabrication of arrays of high-aspect-ratio diamond nanoneedles via maskless ECR-assisted microwave plasma etching. CrystEngComm, 2015, 17, 2791-2800.	1.3	22
197	Feroxyhyte Nanosheets: Iron Vacancies Induced Bifunctionality in Ultrathin Feroxyhyte Nanosheets for Overall Water Splitting (Adv. Mater. 36/2018). Advanced Materials, 2018, 30, 1870272.	11.1	22
198	Electrostatic self-assembly seeding strategy to improve machining performance of nanocrystalline diamond coated cutting tools. Surface and Coatings Technology, 2019, 357, 870-878.	2.2	22

#	Article	IF	CITATIONS
199	A two-photon fluorescent probe for sensitive detection and imaging of Î ³ -glutamyl transpeptidase. Chemical Communications, 2020, 56, 10902-10905.	2.2	22
200	High-Performance CdSe:In Nanowire Field-Effect Transistors Based on Top-Gate Configuration with High-κ Non-Oxide Dielectrics. Journal of Physical Chemistry C, 2010, 114, 4663-4668.	1.5	21
201	From wheat bran derived carbonaceous materials to a highly stretchable and durable strain sensor. RSC Advances, 2017, 7, 22619-22626.	1.7	21
202	Materials with extreme properties: Their structuring and applications. Vacuum, 2012, 86, 575-585.	1.6	20
203	High-throughput intracellular biopsy of microRNAs for dissecting the temporal dynamics of cellular heterogeneity. Science Advances, 2020, 6, eaba4971.	4.7	20
204	Cutting performance of cubic boron nitride-coated tools in dry turning of hardened ductile iron. Journal of Manufacturing Processes, 2020, 56, 158-168.	2.8	20
205	Growth Behavior of Cubic Boron Nitride Films in a Two-Step Process: Changing Bias Voltage, Gas Composition, and Substrate Temperature. Advanced Functional Materials, 2002, 12, 250.	7.8	19
206	Effects at reactive ion etching of CVD diamond. Thin Solid Films, 2000, 368, 222-226.	0.8	18
207	Highly selective recognition of carbenicillin via concerted interactions in 100% aqueous solution. Chemical Communications, 2010, 46, 2435.	2.2	18
208	Controllable Synthesis of Bandgap‶unable CuS _{<i>x</i>} Se _{1â^`<i>x</i>} Nanoplate Alloys. Chemistry - an Asian Journal, 2015, 10, 1490-1495.	1.7	18
209	Surface Transfer Doping of Cubic Boron Nitride Films by MoO ₃ and Tetrafluoro-tetracyanoquinodimethane (F4-TCNQ). ACS Applied Materials & Interfaces, 2015, 7, 9851-9857.	4.0	18
210	A selective fluorescent and colorimetric dual-responses chemosensor for streptomycin based on polythiophene derivative. Spectrochimica Acta - Part A: Molecular and Biomolecular Spectroscopy, 2015, 136, 871-874.	2.0	18
211	Hierarchically nanostructured ZnCo2O4 particles in 3D graphene networks for high-rate and long-life lithium ion batteries. Materials Today Energy, 2019, 12, 46-52.	2.5	18
212	Hypocrellin-Based Multifunctional Phototheranostic Agent for NIR-Triggered Targeted Chemo/Photodynamic/Photothermal Synergistic Therapy against Glioblastoma. ACS Applied Bio Materials, 2020, 3, 3817-3826.	2.3	18
213	Growing cubic boron nitride films at different temperatures. Diamond and Related Materials, 2006, 15, 1155-1160.	1.8	17
214	Effects of ordering degree on the dielectric and ferroelectric behaviors of relaxor ferroelectric Pb(Sc1/2Nb1/2)O3 ceramics. Journal of Applied Physics, 2008, 103, 084124.	1.1	17
215	Quantitative analysis of multiplex-components and double stranded DNA by wide-range surface-enhanced Raman spectroscopy based on ordered Ag/Si nanowire arrays. Journal of Materials Chemistry A, 2014, 2, 10218.	5.2	17
216	Dense diamond nanoneedle arrays for enhanced intracellular delivery of drug molecules to cell lines. Journal of Materials Science, 2015, 50, 7800-7807.	1.7	17

#	Article	IF	CITATIONS
217	Microstructure and tribo-mechanical properties of Ti–B–C nanocomposite films prepared by magnetron sputtering. Surface and Coatings Technology, 2015, 270, 290-298.	2.2	17
218	Synthesis of Boron Nitride Films by Microwave Plasma Chemical Vapor Deposition in Fluorine-Containing Gases. Japanese Journal of Applied Physics, 2001, 40, L570-L572.	0.8	16
219	Recent Progress in Fabrication of Anisotropic Nanostructures for Surface- Enhanced Raman Spectroscopy. Recent Patents on Nanotechnology, 2009, 3, 10-20.	0.7	16
220	Aligned silver nanorod arrays for surface-enhanced Raman spectroscopy. Physica B: Condensed Matter, 2009, 404, 1523-1526.	1.3	16
221	Integrated Nanorods and Heterostructure Field Effect Transistors for Gas Sensing. Journal of Physical Chemistry C, 2010, 114, 7999-8004.	1.5	16
222	Tribological study of boron nitride films. Diamond and Related Materials, 2010, 19, 654-660.	1.8	16
223	A polythiophene-derived ratiometric fluorescent sensor for highly sensitive determination of carbenicillin in aqueous solution. Chemical Communications, 2012, 48, 6818.	2.2	16
224	Sputter deposition of hard quaternary Al–Mg–B–Ti nanocomposite films. Surface and Coatings Technology, 2013, 232, 535-540.	2.2	16
225	Influences of ceramic mating balls on the tribological properties of Cr/a-C coatings with low chromium content in water lubrication. Wear, 2013, 303, 354-360.	1.5	16
226	Controlling Directional Liquid Motion on Micro- and Nanocrystalline Diamond/β-SiC Composite Gradient Films. Langmuir, 2018, 34, 1419-1428.	1.6	16
227	Controllable growth and flexible optoelectronic devices of regularly-assembled Bi2S3 semiconductor nanowire bifurcated junctions and crosslinked networks. Nano Research, 2020, 13, 2226-2232.	5.8	16
228	Structural engineering of sulfur-doped carbon encapsulated bismuth sulfide core-shell structure for enhanced potassium storage performance. Nano Research, 2021, 14, 3545-3551.	5.8	16
229	Plasma-assisted synthesis of nickel-cobalt nitride–oxide hybrids for high-efficiency electrochemical hydrogen evolution. Materials Today Energy, 2021, 21, 100784.	2.5	16
230	Formation and structure of a-C/nanodiamond composite films by prolonged bias enhanced nucleation. Diamond and Related Materials, 2003, 12, 1640-1646.	1.8	15
231	Atomic layer deposition of platinum thin films on anodic aluminium oxide templates as surface-enhanced Raman scattering substrates. Vacuum, 2013, 89, 257-260.	1.6	15
232	Cubic Boron Nitride Films. , 2014, , 607-639.		15
233	Surface doping of nitrogen atoms on graphene via molecular precursor. Applied Physics Letters, 2013, 102, .	1.5	14
234	GaN nanowire arrays by a patterned metal-assisted chemical etching. Journal of Crystal Growth, 2016, 440, 96-101.	0.7	14

#	Article	IF	CITATIONS
235	High-Performance NaVO ₃ with Mixed Cationic and Anionic Redox Reactions for Na-Ion Battery Applications. Chemistry of Materials, 2020, 32, 8836-8844.	3.2	14
236	(001)-textured growth of diamond films on polycrystalline diamond substrates by bias-assisted chemical vapor deposition. Journal of Crystal Growth, 1997, 171, 485-492.	0.7	13
237	Hysteresis in In2O3:Zn nanowire field-effect transistor and its application as a nonvolatile memory device. Applied Physics Letters, 2008, 93, 183111.	1.5	13
238	Transferable, transparent and functional polymer@graphene 2D objects. NPG Asia Materials, 2014, 6, e130.	3.8	13
239	High-Efficiency Cellular Reprogramming by Nanoscale Puncturing. Nano Letters, 2020, 20, 5473-5481.	4.5	13
240	Nearâ€Infrared Hypocrellin Derivatives for Synergistic Photodynamic and Photothermal Therapy. Chemistry - an Asian Journal, 2020, 15, 3462-3468.	1.7	12
241	Photosensitizer doped zeolitic imidazolate framework-8 nanocomposites for combined antibacterial therapy to overcome methicillin-resistant Staphylococcus aureus (MRSA). Colloids and Surfaces B: Biointerfaces, 2020, 190, 110900.	2.5	12
242	Hierarchical trace copper incorporation activated cobalt layered double hydroxide as a highly selective methanol conversion electrocatalyst to realize energy-matched photovoltaic-electrocatalytic formate and hydrogen co-production. Journal of Materials Chemistry A, 2022, 10, 19649-19661.	5.2	12
243	Preferable orientation of turbostratic BN basal planes from an x-ray absorption study. Journal of Materials Research, 2006, 21, 147-152.	1.2	11
244	Deposition of cubic boron nitride films on diamond-coated WC:Co inserts. Diamond and Related Materials, 2009, 18, 1387-1392.	1.8	11
245	Averaging effect on improving signal reproducibility of gap-based and gap-free SERS substrates based on ordered Si nanowire arrays. RSC Advances, 2017, 7, 5297-5305.	1.7	11
246	Hydrogen Evolution Reaction: Nitrogenâ€Doped Grapheneâ€Encapsulated Nickel–Copper Alloy Nanoflower for Highly Efficient Electrochemical Hydrogen Evolution Reaction (Small 48/2019). Small, 2019, 15, 1970260.	5.2	11
247	Reactivity of different tBN environments serving as reaction sites in cBN film deposition. Diamond and Related Materials, 2002, 11, 1416-1421.	1.8	10
248	Growth Characteristics and Texture of Cubic Boron Nitride Films Produced by CVD. Chemical Vapor Deposition, 2002, 8, 262-265.	1.4	10
249	Near-Ultraviolet Light-Emitting Devices Using Vertical ZnO Nanorod Arrays. Journal of Electronic Materials, 2012, 41, 853-856.	1.0	10
250	Profiling MicroRNAs with Associated Spatial Dynamics in Acute Tissue Slices. ACS Nano, 2021, 15, 4881-4892.	7.3	10
251	A chromo- and fluorogenic sensor for probing the cancer biomarker lysophosphatidic acid. Analyst, The, 2012, 137, 1853.	1.7	9
252	Synthesis of high-quality mesoporous silicon particles for enhanced lithium storage performance. Materials Chemistry and Physics, 2016, 173, 89-94.	2.0	9

#	Article	IF	CITATIONS
253	Colorimetric analysis of lipopolysaccharides based on its self-assembly to inhibit ion transport. Analytica Chimica Acta, 2017, 992, 85-93.	2.6	9
254	A novel hypocrellin-based assembly for sonodynamic therapy against glioblastoma. Journal of Materials Chemistry B, 2021, 10, 57-63.	2.9	9
255	Sequencing-free Analysis of Multiple Methylations on Gene-Specific mRNAs. Journal of the American Chemical Society, 2022, 144, 6010-6018.	6.6	9
256	Amphiphilic Diketopyrrolopyrrole Derivatives for Efficient Near-Infrared Fluorescence Imaging and Photothermal Therapy. ACS Omega, 2021, 6, 26575-26582.	1.6	8
257	Trilayer organic narrowband photodetector with electrically-switchable spectral range and color sensing ability. Journal of Materials Chemistry C, 2021, 9, 3814-3819.	2.7	8
258	New Xanthene Dyes with NIRâ€II Emission Beyond 1200Ânm for Efficient Tumor Angiography and Photothermal Therapy. Small, 2022, 18, .	5.2	8
259	Cubic Phase Content and Structure of BN Films from an X-ray Absorption Study. Analytical Chemistry, 2006, 78, 6314-6319.	3.2	7
260	Nearly monodispersed MoS ₂ hierarchical architectures as superior anodes for electrochemical lithium-storage. Nanotechnology, 2019, 30, 415402.	1.3	7
261	Boosting capacity and operating voltage of LiVO3 as cathode for lithium-ion batteries by activating oxygen reaction in the lattice. Journal of Power Sources, 2022, 517, 230728.	4.0	7
262	Extracellular Vesicles for the Diagnosis of Cancers. Small Structures, 2022, 3, 2100096.	6.9	7
263	Surface-Enhanced Raman Scattering Sensor Based on Silver Dendritic Nanostructures. Sensor Letters, 2010, 8, 395-398.	0.4	6
264	Plasma-induced transformation: a new strategy to <i>in situ</i> engineer MOF-derived heterointerface for high-efficiency electrochemical hydrogen evolution. Journal of Materials Chemistry A, 2022, 10, 6596-6606.	5.2	6
265	Ultrathin two-dimensional nickel-organic framework nanosheets for efficient electrocatalytic urea oxidation. Materials Today Energy, 2022, 27, 101024.	2.5	6
266	Theoretical study on misoriented diamond nucleations on Si(001) surface. Diamond and Related Materials, 1999, 8, 1418-1422.	1.8	5
267	Modulation of surface-enhanced Raman spectra by depth selective excitation of embedded indium tin oxide nanoisland arrays. Journal Physics D: Applied Physics, 2011, 44, 215305.	1.3	5
268	Lithiophilicity conversion of carbon paper with uniform Cu2+1O coating: Boosting stable Li-Cu2+1O-CP composite anode through melting infusion. Chemical Engineering Journal, 2020, 388, 124238.	6.6	5
269	Epitaxial growth of structure-tunable ZnO/ZnS core/shell nanowire arrays using HfO ₂ as the buffer layer. Nanoscale, 2022, 14, 7579-7588.	2.8	5
270	The contribution of H + ion etching during the initial deposition stage to the orientation grade of diamond films. Thin Solid Films, 1999, 348, 84-89.	0.8	4

#	Article	IF	CITATIONS
271	Trace detection of multiwalled carbon nanotubes using Raman-enhancing silver nanocap arrays. Journal Physics D: Applied Physics, 2010, 43, 455302.	1.3	4
272	Visible light photodegradation of rhodamine B over VDF/CTFE copolymer-templated crystalline mesoporous titania. Research on Chemical Intermediates, 2012, 38, 2383-2391.	1.3	4
273	Nanotechnology: Advanced Materials and Nanotechnology for Drug Delivery (Adv. Mater. 31/2014). Advanced Materials, 2014, 26, 5576-5576.	11.1	4
274	Study on l–V characteristics of diamond films synthesized by D.C. arc discharge plasma chemical vapour deposition. Thin Solid Films, 1991, 205, 39-42.	0.8	3
275	Electrical and photoconductive properties of boron-doped potycrystalline diamond films. Journal of Materials Research, 1995, 10, 2350-2354.	1.2	3
276	Batteries: Electrochemically Stable Sodium Metalâ€īellurium/Carbon Nanorods Batteries (Adv. Energy) Tj ETQqO	0 0 rgBT / 10:2	Ovgrlock 10 T
277	Ultrasoundâ€Enhanced Selfâ€Exciting Photodynamic Therapy Based on Hypocrellin B. Chemistry - an Asian Journal, 2021, 16, 1221-1224.	1.7	3
278	Vapor phase epitaxy of PbS single-crystal films on water-soluble substrates and application to photodetectors. Nano Research, 2022, 15, 5402-5409.	5.8	3
279	Diamond and cubic boron nitride: synthesis and electronic applications. , 0, , .		2
280	Experimental and theoretical investigation of the effects of sample size on copper plasma immersion ion implantation into polyethylene. Journal of Applied Physics, 2007, 101, 113302.	1.1	2
281	Solar Cells: Surface Engineering of ZnO Nanostructures for Semiconductor‣ensitized Solar Cells (Adv. Mater. 31/2014). Advanced Materials, 2014, 26, 5575-5575.	11.1	2
282	Intracellular Delivery: Diamondâ€Nanoneedleâ€Arrayâ€Facilitated Intracellular Delivery and the Potential Influence on Cell Physiology (Adv. Healthcare Mater. 10/2016). Advanced Healthcare Materials, 2016, 5, 1116-1116.	3.9	2
283	Time-dependent photoconductive properties of polycrystalline diamond films with different boron concentration. Materials Letters, 1995, 25, 17-20.	1.3	1
284	The Origin of Mis-Oriented Diamond Grains Nucleated Directly on (001) Silicon Surface. Materials Research Society Symposia Proceedings, 1998, 529, 139.	0.1	1
285	Hot spots in silver nano-dendrites fabricated by self-selective electroless plating. , 2010, , .		1
286	Silver surface-enhanced raman scattering substrates prepared by a nanofabrication process using Electron Beam Lithography and magnetron sputtering. , 2013, , .		1
287	Plasmon-enhanced luminescence in MEH-PPV coupled silver nanoantenna arrays and the potential for photovoltaics. , 2010, , .		0
288	Controlled assembly of sliver nanocap arrays with tunable gaps for molecular sensing using SERS. , 2010, , .		0

#	Article	IF	CITATIONS
289	Surface-enhanced Raman Scattering Substrates Prepared by Magnetron Sputtering Using Anodized Titanium Oxide Nanotube Ends as Template. , 2013, , .		Ο
290	Metal-Enhanced Cellular Fluorescence Imaging on Silver Nano-Arrays Prepared by Electron-Beam Lithography and Magnetron Sputtering. , 2014, , .		0